Spatially-Resolving Nanoscopic Structure and Excitonic-Charge-Transfer Quenching in Molecular Semiconductor Heterojunctions

David M. Adams, Josef Kerimo, Eric J. C. Olson, Arie Zaban,† Brian A. Gregg,† and Paul F. Barbara*

Contribution from the Department of Chemistry, University of Minnesota, 207 Pleasant Street SE, Minneapolis, Minnesota 55455, and The National Renewable Energy Lab, 1617 Cole Boulevard, Golden, Colorado 80401

Received May 29, 1997[⊗]

Abstract: Near-field scanning optical microscopy (NSOM) and scanning force microscopy have been employed to spatially resolve the complex morphologies, spectroscopy, and charge transfer induced fluorescence quenching efficiencies of a (perylene phenethylimide)/(titanyl phthalocyanine) bilayer (PPEI/TiOPc). The PPEI/TiOPc bilayer is a typical example of a *n*-like/*p*-like molecular semiconductor heterojunction, which is a common component in photocells, LEDs, and other devices. NSOM-polarized fluorescence and transmission data—and separate bulk X-ray diffraction and spectroscopic measurements—on PPEI/TiOPc bilayers and PPEI and TiOPc single layers has lead to a nanoscopic and mesoscopic picture of how vacuum deposition and subsequent solvent-vapor-annealing controls the local structure of these films. The layers and bilayers are highly organized, containing localized crystalline regions which are preferentially oriented relative to the substrate and PPEI/TiOPc interface. In highly annealed bilayers, only a small fraction of the area of the interface makes good contact between the bilayers, and the contact regions are less than 100 nm^2 in most cases. The consequences of the observed morphology on the charge separation efficiencies at the interface is examined. It is shown that exciton migration both perpendicular and parallel to the molecular interface are involved in the charge separation mechanism. Extended methylene chloride, solvent-vapor-annealing of PPEI films produces long needle-like PPEI crystals with a range of sizes, as follows: width (50−200 nm), length (1000−2000 nm), and height (50−200 nm). Annealing of the TiOPc yields nanocrystallites that are preferentially oriented relative to the interface with a height in the range of 10−100 nm and widths in the range of <10 nm to 30 nm.

Introduction

There is tremendous activity in the use of molecular semiconductor heterojunctions in optical and electronic devices, including light-emitting-diode displays, chemical sensors, and solar cells.[1−8] For example, consider a typical solar cell device, as shown in Figure 1, in which the semiconductor heterojunction is comprised of an interface between *n*-like and *p*-like molecular semiconductor layers (*n*-MSL and *p*-MSL). Light absorption in the *n*-MSL (typically a perylene derivative) results in the production of mobile singlet excitons which diffuse to the perylene/*p*-MSL interface and then create an electron-hole pair *across the interface* by electron transfer, i.e. generation of charge carriers. The charge carrier generation process is effected by the rates and efficiencies of many "primary processes" including exciton diffusion/migration to the interface, kinetics of electron transfer across the interface between molecular pairs, dissociation of the charge transfer state into free carriers at the interface, and the "energy wasting", radiative and radiationless decay of excitons *en route* to the interface.[9−13] It should be emphasized that the efficiencies and rates of these various photophysical processes are believed to be a strong function of the complex morphologies of the perylene layer, the *p*-MSL layer, and the interfacial region. Indeed, the interface structure depicted in Figure 1 is highly oversimplified since the morphology of the individual layers and interfacial regions in real devices are known to be highly structured on the meso- and nanoscale which implies highly anisotropic electrical and photophysical properties.

Thin film morphologies are a strong function of the methods and conditions of film preparation, including vacuum deposition, spin-casting, etc. Film morphologies can also be dramatically altered by post-deposition-processing, including solvent-vapor-annealing, thermal-annealing, solvent "pasting", etc., which leads to highly nanostructured crystalline films with a high degree of order.[3,4,14−16] These post-deposition-processing techniques are

* Author to whom correspondence should be addressed.
† NREL.
⊗ Abstract published in *Advance ACS Abstracts,* October 15, 1997.

(1) Reinecker, P.; Haken, H.; Wolf, H. C. E. *Organic Molecular Aggregates*; Springer Verlag: Berlin, 1983.
(2) Simon, J.; Andre, J. J. *Molecular Semiconductors*; Springer Verlag: Berlin, 1985.
(3) Law, K.-Y. *Chem. Rev.* **1993**, *93*, 449.
(4) Borsenberger, P. M.; Weiss, D. S. *Organic Photoreceptors for Imaging Systems*; Marcel Dekker: New York, 1993.
(5) Wohrle, D.; Meissner, D. *Adv. Mater.* **1991**, *3*, 129.
(6) Wohrle, D.; Kreienhoop, L.; Schnurpfiel, G.; Elbe, J.; Tennigkeit, B.; Hiller, S.; Schlettwein, D. J. *Mater. Chem.* **1995**, *5*, 1819.
(7) Danziger, J.; Dodelet, J.-P.; Lee, P.; Nebesny, K. W.; Armstrong, N. R. *Chem. Mater.* **1991**, *3*, 821.
(8) Burrows, P. E.; Shen, Z.; Bulovic, V.; McCarty, D. M.; Forrest, S. R.; Cronin, J. A.; Thompson, M. E. *J. Appl. Phys.* **1996**, *79*, 7991.
(9) Geacintov, N.; Pope, M.; Kallman, H. *J. Chem. Phys.* **1966**, *45*, 2639.
(10) Popovic, Z. D.; Hor, A.-M.; Loutfy, R. O. *Chem. Phys.* **1988**, *127*, 451.
(11) Gregg, B. A.; Fox, M. A.; Bard, A. J. *J. Phys. Chem.* **1990**, *94*, 1586.
(12) Gregg, B. A.; Kim, Y. I. *J. Phys. Chem.* **1994**, *98*, 2412.
(13) Gregg, B. A. *Appl. Phys. Lett.* **1995**, *67*, 1271.
(14) Debe, M. K.; Kam, K. K.; Liu, J. C.; Poirier, R. J. *J. Vac. Sci. Tech. A* **1988**, *6*, 1907.
(15) Tamizhmani, G.; Dodelet, J. P.; Cote, R.; Gravel, D. *Chem. Mater.* **1991**, *3*, 1046.
(16) Gastonguay, L. G.; Veilleux, G.; Cote, R.; Saint-Jacques, R. G.; Dodelet, J. P. *J. Electrochem. Soc.* **1992**, *139*, 337.

S0002-7863(97)01777-0 CCC: $14.00

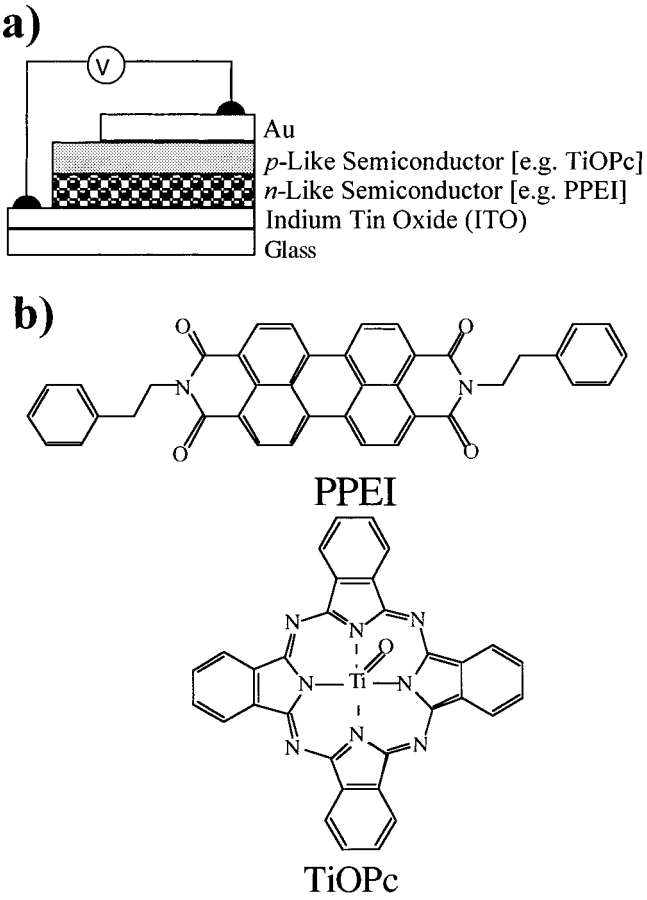

Figure 1. (a) Schematic drawing of a typical geometry for a molecular semiconductor based heterojunction photovoltaic device. (b) Chemical structures of perylene phenethylimide (PPEI) and titanyl phthalocyanine (TiOPc).

known to improve the electrophotographic,[3,4] photovoltaic,[17−20] photoconductive,[21] and photoelectrochemical[15,16,22] properties of thin film devices in many cases, including well established industrial applications.[23,24] This improved performance has been attributed to longer range exciton migration, improved optical properties, improved photoconductivities, alterations of the optical and/or electronic band structures, and other factors. In contrast, in certain cases, solvent-vapor-annealing over extended periods has been reported to degrade photoconductivity and other properties (especially for thin bilayers).[20] It would be beneficial to develop a detailed morphologically-based understanding of the apparently conflicting results on the effect of solvent annealing on the various properties of the heterojunctions.

Despite the extensive research that shows that nanoscopic and mesoscopic structure can dramatically effect device performance, *direct spatially resolved photophysical measurements* designed to probe the structural dependence of the photophysical behavior of these bilayer assemblies have rarely been pursued. Indeed, much of the current understanding of perylene/*p*-MSL photophysics has been inferred from bulk spectroscopic and thin-film conductivity techniques, in conjunction with nonspectroscopic structural techniques such as scanning electron microscopy (SEM)[14−16,25] and atomic force microscopy (AFM).[6]

The present study, in contrast, utilizes the high topographical and optical/spectroscopic resolution of near-field scanning optical microscopy (NSOM) to investigate a typical bilayer heterojunction, namely, perylene phenethylimide (PPEI)/ titanyl phthalocyanine (TiOPc) (Figure 1). NSOM is a high resolution scanning probe technique which produces simultaneous topographical (resolution ∼10 nm) and optical/spectroscopic images (resolution ≥ 30 nm). It has been shown to be a unique tool in the investigation of the morphology of organic photoactive nanostructured thin film materials, including locally aggregated conjugated-polymer thin films, complex thin film assemblies of fluorescent molecules such as porphyrin wheels and fibrous j-aggregates, and organic nanocrystals.[26−31] In particular, near-field optical *spectroscopy* (both transmission and fluorescence) has been used to effectively probe the local electronic structure of molecular systems via the local electronic spectra (emission, absorption) of these materials. Furthermore, NSOM spectroscopy with polarized light and polarized detection schemes has been shown to be an efficient and extraordinarily sensitive tool for the determination of the local molecular orientation of nanostructured thin films.[32,33]

In this paper, fluorescence NSOM, transmission NSOM, and simultaneous scanning force microscopy are used to determine the PPEI/TiOPc bilayer morphology over a range of distance scales form the molecular to the macroscopic. Additionally, the effect of the observed morphology on the charge generation efficiency is inferred by spatially resolving the TiOPc-induced quenching of the PPEI charge transfer-exciton-fluorescence. Since the primary quenching mechanism of excitons at the PPEI/TiOPc interface is apparently charge separation,[10] fluorescence quenching can be used in bulk studies as an indirect measure of charge transfer at the interface.[25] The NSOM data in this paper leads to *a nanoscopic understanding* of how vacuum-deposition and solvent-vapor-annealing controls the complex morphologies and photophysical properties of a bilayer, and in particular, why solvent annealing can alternately improve or degrade charge generation efficiency of perylene/*p*-MSL heterojunctions depending on film preparation conditions.

Experimental Section

Materials. Perylene phenethylimide, PPEI (structure is shown in Figure 1b) was synthesized and purified as reported previously.[20] Titanyl phthalocyanine (TiOPc) (Figure 1b) was purchased from H. W. Sands Corp. Glass microscope cover slips substrates were dehydrated prior to use by baking at 150 °C for at least 1 h. They were then transferred directly to the evaporation chamber. PPEI and TiOPc were separately evaporated in a vacuum at $\sim 10^{-7}$ Torr onto substrates at room temperature by a method previously described.[20]

(17) Hor, A.-M.; Loutfy, R. O. *Thin Solid Films* **1983**, *106*, 291.
(18) Loutfy, R. O.; Hor, A.-M.; Kazmaier, P.; Tam, M. *J. Imag. Sci.* **1989**, *33*, 151.
(19) Tsuzuki, T.; Kuwabara, Y.; Noma, N.; Shirota, Y. *Jpn. J. Appl. Phys.* **1996**, *35*, L447.
(20) Gregg, B. A. *J. Phys. Chem.* **1996**, *100*, 852.
(21) Saito, T.; Sisk, W.; Kobayashi, T.; Suzuki, S.; Iwayanagi, T. *J. Phys. Chem.* **1993**, *97*, 8026.
(22) Klofta, T. J.; Rieke, P. C.; Linkous, C. A.; Buttner, W. J.; Nanthakumar, A.; Mewborn, T. D.; Armstrong, N. R. *J. Electrochem. Soc.* **1985**, *132*, 2134.
(23) Borsenberger, P. M.; Regan, M. T.; Staudenmayer, W. J. US Patent 4578334, 1986.
(24) Borsenberger, P. M.; Regan, M. T.; Staudenmayer, W. J. US Patent 4618560, 1986.
(25) Gregg, B. A.; Sprague, J.; Peterson, M. W. *J. Phys. Chem., in press.*
(26) Vanden Bout, D. A.; Kerimo, J.; Higgins, D. A.; Barbara, P. F. *Acc. Chem. Res.* **1997**, *30*, 204.
(27) Betzig, E.; Trautman, J. K. *Science* **1992**, *257*, 189.
(28) Pohl, D. W. *Optical and Electron Microscopy* **1991**, *12*, 243.
(29) Lieberman, K.; Harush, S.; Lewis, A.; Kopelman, R. *Science* **1990**, *247*, 59.
(30) Heinzelmann, H.; Huser, T.; Lacoste, T.; Güntherodt, H.-J.; Pohl, D.; Hecht, B.; Novotny, L.; Martin, O. J. F.; Hafner, C. V.; Baggenstos, H.; Wild, U. P.; Renn, A. *Opt. Eng. (Bellingham, Wash.)* **1995**, *34*, 2441.
(31) Buratto, S. K. *Curr. Opin. Solid-State Mater. Sci.* **1996**, *1*, 485.
(32) Vaez-Iravani, M.; Toledo-Crow, R. *Appl. Phys. Lett.* **1993**, *63*, 138.
(33) Higgins, D. A.; Vanden Bout, D. A.; Kerimo, J.; Barbara, P. F. *J. Phys. Chem.* **1996**, *100*, 13794.

Various films were prepared with single layers of TiOPc and PPEI, as well as PPEI/TiOPc bilayers. In certain cases PPEI only layers and PPEI/TiOPc bilayers were prepared on the same substrate to aid in making comparisons between the different types of films. The films were solvent-vapor-annealed in a methylene chloride/air environment at room temperature for the various times described below.

X-ray Diffraction. Thin film X-ray diffraction measurements of the solvent-vapor-annealed films were recorded on a Siemens D-500 diffractometer from 2θ angles of 5° to 35°, step size = 0.05°, and at collection times of 90 s per step. Diffraction data were corrected for the scattering of the glass cover slips. For further details see Supporting Information S1−S5.

NSOM Measurements. The static and time-resolved NSOM measurements were performed on a modified Topometrix Aurora NSOM using homemade NSOM probes. The apparatus and analogous experimental methods have been described in detail elsewhere.[27,34,35] NSOM measurements were reproduced on numerous occasions with different NSOM tips and in different regions of the sample, or with different samples. The results were observed to be highly reproducible and not subject to artifacts due to sample heating by the NSOM probe or photolysis of the samples by the near-field excitation.

Results and Discussion

Overview. The two major issues in this paper are (i) the effects of solvent-vapor-annealing on the morphologies of the PPEI/TiOPc heterojunction and (ii) the impact of the modified morphology on the efficiency of the PPEI exciton quenching at the PPEI/TiOPc interface. Toward these goals, a variety of PPEI, TiOPc, and PPEI/TiOPc bilayer thin films were prepared by vacuum deposition. Vacuum deposition of organics under the conditions described herein, produces amorphous flat layers that conform to the substrate or underlayer (which itself may be rough). The thicknesses reported in this paper correspond to the film thickness after deposition only, i.e. before solvent-vapor-annealing.

The complex morphologies of the PPEI, TiOPc, and PPEI/TiOPc thin films, at various stages of solvent-vapor-annealing, have been characterized by bulk spectroscopy and X-ray diffraction methods. More importantly, the morphologies of the films have been *directly* resolved *spatially* by a variety of fluorescence and transmission NSOM experiments as portrayed in Figure 2. Polarized spectroscopic NSOM experiments have been employed to obtain a detailed, nanoscopic picture of the PPEI/TiOPc molecular interface. Thin film PPEI/TiOPc bilayers have been studied to examine how solvent-vapor-annealing alters the PPEI morphology away from the PPEI/TiOPc interface. Finally, the nanoscale details of the PPEI/TiOPc charge generation process have been inferred from spatially resolved static and time-resolved fluorescence experiments.

Bulk Spectroscopy of the Films. Much of the data presented in this paper involves optical excitation at 488 nm of the PPEI layer of a PPEI/TiOPc bilayer and associated quenching of this fluorescence by charge transfer across the PPEI/TiOPc interface. The electronic absorption spectrum of a 30 nm film of PPEI vapor-annealed in CH_2Cl_2 for 30 min is shown in Figure 3. The vapor-annealed films show two absorption maxima at 460 and 610 nm. The solution electronic absorption spectrum of many perylene derivatives show well structured vibronic transitions to the S_1 state, where the 0-0 transition is located at ~530 nm. The splitting of this absorption band in the solid state, into higher and lower energy components, respectively, occurs as the amorphous film is vapor-annealed.[20] Vapor-annealing of the films beyond 30 min does not result in further significant changes in the spectrum. Large shifts in energy of the optical absorption bands are evidence of the strong intermolecular interactions which occur in the solid state. The characteristics of the vapor-annealed PPEI thin film absorption are similar to those observed in related thin films of perylene tetracarboxylic acid dianhydride (PTCDA).[36,37] The high energy band in

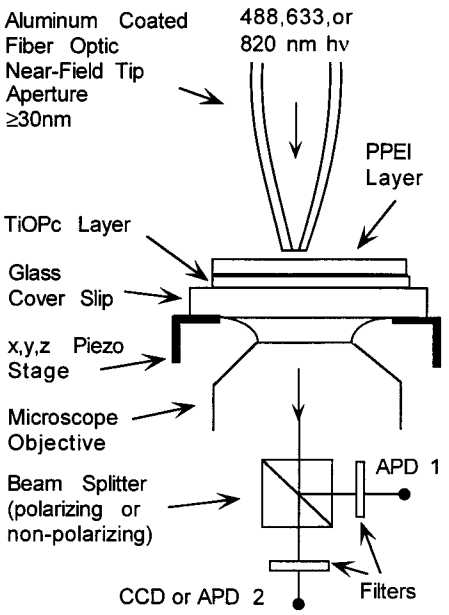

Figure 2. The experimental geometry used in the present study. The aluminum-coated fiber optic probe (~70 nm Al coating, >30 nm aperture) and oil emersion microscope objective are held in fixed positions relative to the sample. The sample is brought into the near field of the NSOM probe and is held within 5−10 nm (±1 nm) of the probe with the shear-force feed-back mechanism. The sample stage is scanned in the *X,Y* plane, and the tip-sample distance in the *Z* direction is regulated by moving the sample. An oil immersion objective is used to collect transmitted and/or fluorescence from the sample which is sent to a beam splitter. The signal can be simultaneously detected by two separate avalanche photodiode detectors (APD) in conjunction with a charge-coupled device (CCD) camera. Filters are placed prior to the detectors to block the laser excitation and/or fluorescence.

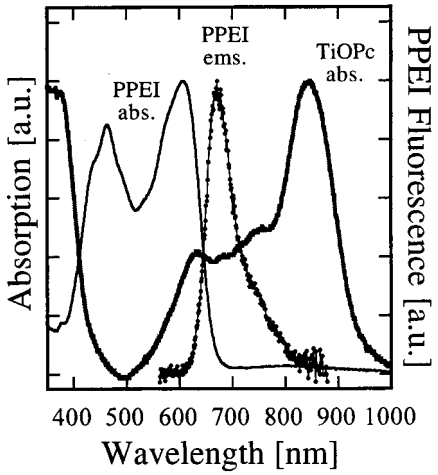

Figure 3. Electronic absorption spectra of CH_2Cl_2 vapor-annealed PPEI (thin solid line) and TiOPc (thick solid line) thin films. The near-field fluorescence spectrum of a single PPEI nanocrystal is plotted as a dotted line. The optical absorption in arbitrary units (left axis) and fluorescence intensity in arbitrary units (right axis) are plotted versus wavelength (λ) in units of nanometers.

(34) Reid, P. J.; Higgins, D. A.; Barbara, P. F. *J. Phys. Chem.* **1996**, *100*, 3892.

(35) Vanden Bout, D. A.; Kerimo, J.; Higgins, D. A.; Barbara, P. F. *J. Phys. Chem.* **1996**, *100*, 11843.

(36) Bulovic, V.; Burrows, P. E.; Forrest, S. R.; Cronin, J. A.; Thompson, M. E. *Chem. Phys.* **1996**, *210*, 1.

(37) Bulovic, V.; Forrest, S. R. *Chem. Phys.* **1996**, *210*, 13.

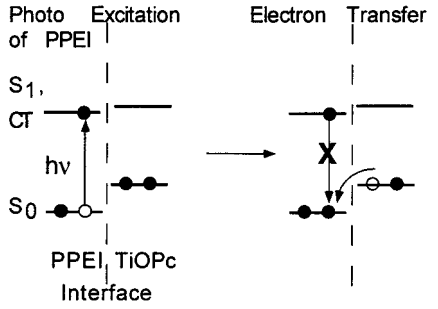

Figure 4. Schematic representation of the charge separation process at the interface. The horizontal lines represent the approximate relative energy orderings of the highest occupied molecular orbital (HOMO) and lowest unoccupied molecular orbital (LUMO) of the PPEI and TiOPc molecules at the interface. Photoexcitation of the PPEI surface leads to creation of Frenkel like (S_1) or charge transfer (CT) excitonic states which diffuse to the interfacial region where charge separation occurs by electron transfer from the HOMO of TiOPc molecule to the HOMO of the PPEI molecule. The efficiency of charge carrier generation in molecular semiconductor heterojunctions is influenced by exciton diffusion to the interface, kinetics of electron transfer across the interface between molecule pairs (driving force and reorganization energies), and dissociation probability of charge separated species into free carriers.

PTCDA has been assigned as the transition to a so-called S_1 Frenkel-like state (i.e. the excitation is confined to the monomer), while the low energy band has been assigned to a charge transfer (CT) excitonic state with a radius of 12 Å involving charge transfer over more than one perylene molecule. The near-field excited fluorescence spectrum of a single nanocrystal of PPEI is also shown in Figure 3. Fluorescence of the vapor-annealed PPEI film occurs from the lowest energy excited sate, namely the CT state.

The designation S_1 Frenkel-like state is a misnomer since the CT band of the crystal is actually the lowest energy excited singlet state. Nevertheless, the so-called S_1 Frenkel-like state does correspond to S_1 of perylenes in solution, i.e. for which the CT is absent and the lowest excited state is a $\pi-\pi^*$ in plane, long axis polarized transition.[38,39]

The visible Q-band absorption of phthalocyanines occurs in the 600−750 nm range and arises from the $\pi-\pi^*$ in plane polarized charge transfer transition of the phthalocyanine ring system.[3] The electronic absorption spectrum of a 10 nm film of TiOPc-annealed in methylene chloride vapor for 24 h is shown in Figure 3. The annealed TiOPc films show a broad absorption from 600−950 nm with maxima occurring at 610 and 860 nm. The evolution of the optical absorption spectrum of TiOPc upon vapor-annealing with CH_2Cl_2 is qualitatively similar to the evolution observed in PPEI films. The low energy band at 860 nm has been assigned as a charge transfer excitonic state.[21]

The mechanism of charge separation at the interface of a PPEI/TiOPc bilayer assembly is schematically represented in Figure 4. Absorption by the PPEI layer into the S_1 Frenkel exciton band near 488 nm efficiently produces CT excitons by a radiationless decay mechanism. In the absence of a TiOPc layer, the PPEI layer is highly fluorescent. At the interface, exciton dissociation occurs by injection of an electron into the perylene layer and a hole into TiOPc layer (i.e. electron transfer from TiOPc to PPEI). Thus, the electron transfer process at the PPEI/TiOPc interface is an efficient quenching mechanism for the CT fluorescence of the PPEI layer.

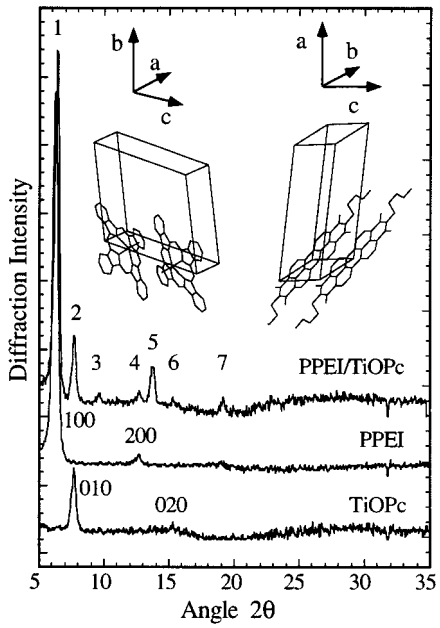

Figure 5. X-ray scattering data for the CH_2Cl_2 vapor-annealed thin films. (a) PPEI/TiOPc on glass. (b) PPEI only on glass. (c) TiOPc only on glass. The diffraction intensity is plotted versus diffraction angle (2θ).

X-ray Diffraction Measurements. X-ray diffraction measurements on the vapor-annealed films of TiOPc, PPEI, and PPEI/TiOPc were performed in order to ascertain the molecular order and orientation (Figure 5) in the films. A detailed description of the data and analysis is given in Supporting Information S1−S5. TiOPc films in the present study have been assigned to the phase II polymorph previously reported.[40] The *b*-axis of the unit cell must lie vertical to the surface for these reflections to be observed. The inset of Figure 5 displays the unit cell of the phase II polymorph of TiOPc where the *b*-axis is plotted in the vertical direction. In order to illustrate the molecular orientation relative to the substrate, a stereoplot of the TiOPc unit cell is plotted in Figure 6a, where the *a*,*c*-plane of the unit cell is plotted in the plane of the paper. Two more molecules have been added to the unit cell in order to illustrate the molecular packing in the crystal. The phthalocyanine molecules orient edge on to the substrate and resemble slightly "tipped-over domino" rows. Within a given row, TiOPc molecules have identical orientation. The oxygen groups of phthalocyanines in a given row are aligned oppositely to the neighboring rows.

It will be shown below that the solvent-annealed PPEI layer exhibits long needle-like crystals with a single apparent morphology. The only reported crystal structure of PPEI has a *C*2/*c* space group with four molecules per unit cell, and half the molecules arranged orthogonal to the other half.[41] The X-ray diffraction pattern of a 50 nm PPEI thin film annealed in methylene chloride for 48 h is shown in Figure 5. The positions of the diffraction peaks of the vapor-annealed PPEI film in the present study do not correspond to any of the diffraction peaks which are expected for the *C*2/*c* structure, and thus it is unlikely that this morphology is present in the samples described in this paper.

Current studies are in progress to obtain a single crystal structure of the PPEI from methylene chloride solution suitable for single crystal X-ray diffraction. Many perylene derivatives crystallize in the $P\bar{1}$ space group with one molecule per unit

(38) Adachi, M.; Yukichi, M.; Nakamura, S. *J. Phys. Chem.* **1995**, *99*, 19.
(39) Kazmaier, P. M.; Hoffmann, R. *J. Am. Chem. Soc.* **1994**, *116*, 9684.
(40) Hiller, W.; Strahle, J.; Kobel, W.; Hanack, M. *Z. Kristallogr.* **1982**, *59*, 173.
(41) Hadicke, E.; Graser, F. *Acta Crystallogr.* **1986**, *C42*, 189.

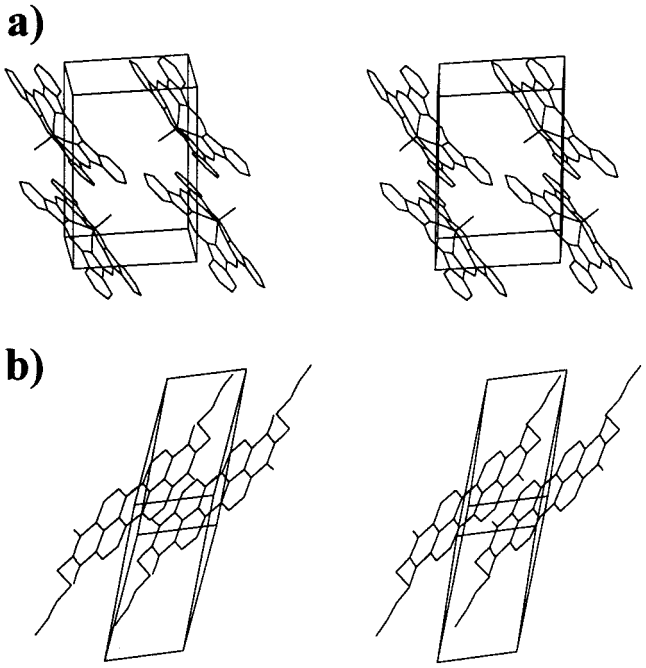

Figure 6. Stereoplots of the unit cells of (a) TiOPc and (b) perylene methylpropylimide (PMPI), an isostructural analog of PPEI. The view depicts the orientation of the unit cells relative to the substrate (plane of the paper) as derived from the X-ray diffraction data.

cell.[41] Perylene 3-methoxy propylimide, PMPI, and PPEI have similar molecular dimensions. Furthermore, thin films of PMPI have nearly identical optical absorption characteristics to those of the annealed PPEI films in the present study.[42,43] It is likely that the methylene chloride vapor-annealing process produces a crystalline form of PPEI which is nearly identical to the $P\bar{1}$ structure of PMPI. Figure 6b shows a stereoplot of PMPI where the view is perpendicular to the *b*,*c*-face of the unit cell which lies in the plane of the paper. The vapor-annealed PPEI crystals likely have this orientation of the unit cell relative to the substrate where the *b*,*c*-face of the unit-cell is parallel to the surface. The *b*-axis of the unit cell lies along the long axis of the crystal. Moreover the long axis of the perylene ring system is tilted ∼45° off of the *b*-axis. Such an orientation of the perylene is expected to produce highly anisotropic absorption of light.

NSOM Investigation of the Morphologies of Vacuum-Deposited/Solvent-Vapor-Annealed TiOPc and PPEI Single Layers and Heterojunctions. (i) Annealed TiOPc (10 nm). The topographical image of a 10 nm TiOPc film that was annealed for 24 h is shown in Figure 7a. The image shows that the initially amorphous film has restructured to a highly porous film of nanocrystallites ranging in height from the level of the substrate (0 nm) to over 100 nm. The flat profile of the fiber probe is responsible for making the TiOPc crystals to appear bigger in the film plane due to a so-called tip-artifact. Indeed, topographical images with a conventional AFM tip of similar films shows that more than half of the film area is void of TiOPc and at the level of the substrate.[44] These images reveal sharp pointed TiOPc nanocrystals which are not fully resolved even with sharp AFM tips. The typical in-plane cross-sections of these TiOPc nanocrystals range from <10 nm to 30 nm. The heights of the crystals, in contrast, are not distorted by the shear-force images and range up to 100 nm.

(42) Graser, F.; Hadicke, E. *Liebigs Ann. Chem.* **1984**, 483.
(43) Graser, F.; Hadicke, E. *Liebigs Ann. Chem.* **1980**, 1994.
(44) Conboy, J. C.; Barbara, P. F. Work in progress.

(ii) Annealed PPEI (30 nm) and PPEI/TiOPc (30 nm/10 nm). Bilayer assemblies of PPEI/TiOPc were made by first evaporating 10 nm of TiOPc onto half of the glass substrate and subsequently vapor-annealing this film in methylene chloride for 24 h. 30 nm of PPEI was then evaporated onto the vapor-annealed TiOPc film, such that a single glass substrate contained PPEI on a TiOPc layer on one half and PPEI on the bare glass on the other. These slides were then subsequently vapor-annealed in methylene chloride for an additional 30 min. The PPEI/TiOPc region of the films partially retains the topography of the TiOPc underlayer layer (Figure 7b). The polarized near-field fluorescence images of this film obtained with 488 nm photoexcitation (Figures 7c,d) display large intensity variations in fluorescence and highly polarized regions of fluorescence of the PPEI overlayer. These regions of polarized emission are attributed to crystalline domains of PPEI which reside on the crystalline TiOPc surface. The size of many of the PPEI domains is smaller than the near-field optical resolution of ∼70 nm. The variations in fluorescence intensity are attributable to local variations in PPEI concentration. *It is likely that crystallization of PPEI is aided by the TiOPc surface and occurs preferentially on the TiOPc crystals.*

For comparison, the topographical and fluorescence images of the PPEI only region of the sample is shown in Figures 7e−g. These PPEI only regions show much less topographical variation than PPEI/TiOPc. Although the images show some polarization dependent variations in fluorescence intensity, the films display much more uniform PPEI fluorescence over the entire scan region than PPEI/TiOPc. It is likely that in contrast to PPEI films on TiOPc, smaller crystalline domains of PPEI form on the bare glass and cover the surface more uniformly.

(iii) Thick PPEI (300 nm) with Moderate Annealing. The topographical image of Figure 7h and fluorescence image Figure 7i (different region) show the remarkable features of a 300 nm vacuum-deposited PPEI film after extended annealing in methylene chloride. The annealing process creates large needle-like crystals of PPEI which range from hundreds of nanometers to microns in their long direction. Previous investigations have utilized solvent-annealed thicker films such as these to study the photovoltaic effect in PPEI/TiOPc, and also to measure the exciton diffusion lengths in PPEI/*p*-MSL assemblies.[20,25] For our purposes of characterizing the interfacial region, these thicker films were not appropriate, since the fluorescence images were uninterpretable due to competing near-field and far-field effects inherent when studying thicker films with NSOM. Purposefully thin films of PPEI were used in the present study in order to obtain, after solvent annealing, isolated crystals of PPEI which lie on the TiOPc surface.

It is important to note that thick PPEI films are nearly continuous, i.e. lacking open regions to the substrate level (Figure 7h). Additionally the largest PPEI crystals are at the exposed face of the film. This implies, as might be expected, that the annealing process in a thick film is most dramatic at the exposed face. Thus, in a PPEI/TiOPc bilayer with a thick exposed PPEI layer, short-to-moderate time solvent-vapor-annealing times would be expected to primarily alter the top of the PPEI layer, while having much less if any impact on the PPEI/TiOPc molecular interface.

(iv) PPEI and PPEI/TiOPc with Extended Annealing. The mechanism of the solvent-vapor-annealing process is not well understood. The substrate that contained the bilayer assembly PPEI/TiOPc and PPEI on bare glass and whose topographical and fluorescence images are shown in Figures 7b−g was subjected to 48 h more of solvent vapor-annealing. Figure 8a dramatically displays the topographical changes which occur as the initially amorphous film is subjected to extended vapor-

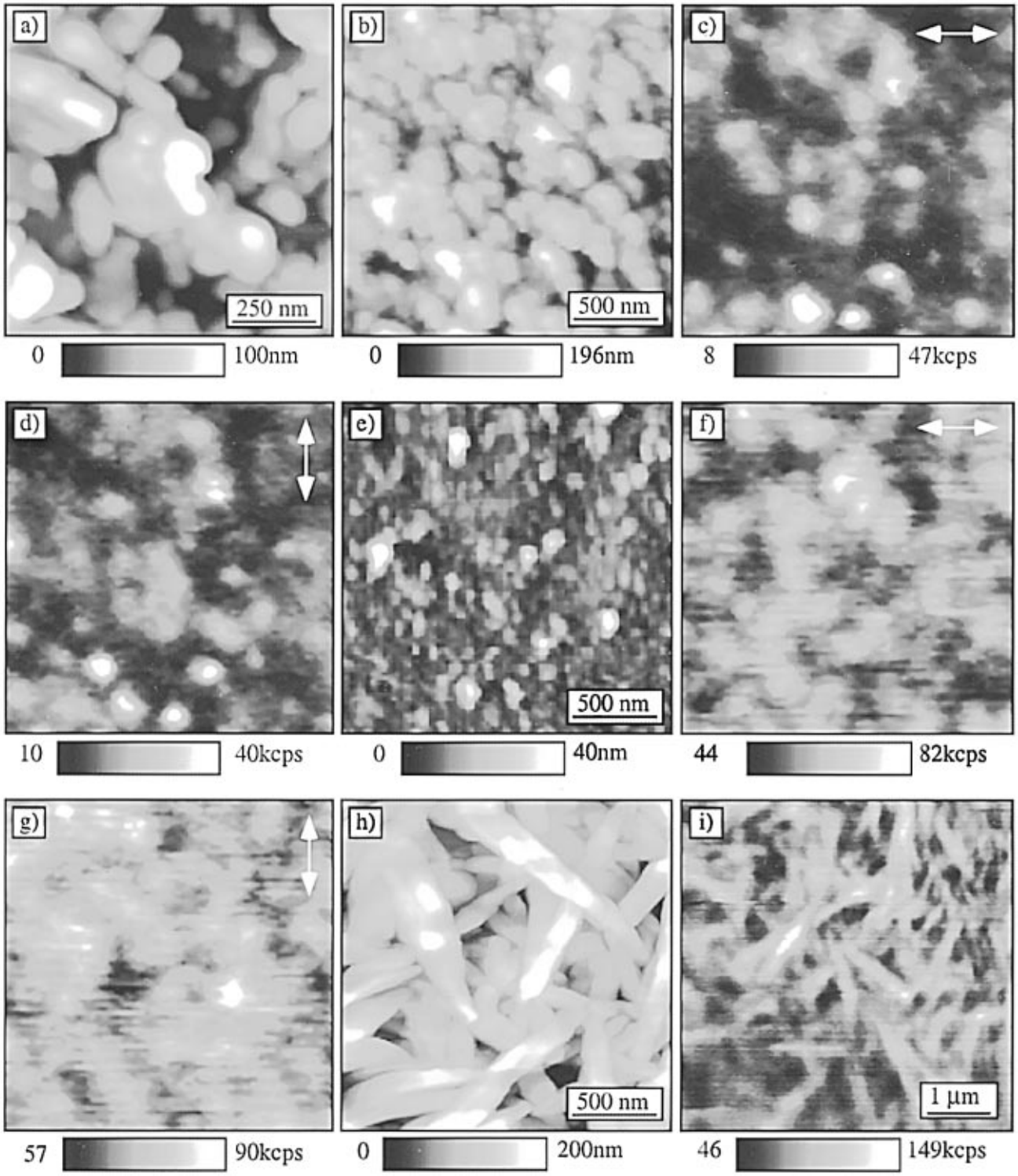

Figure 7. (a) Topographic image of a 10 nm TiOPc thin film which was vapor-annealed in CH_2Cl_2 for 24 h. Topographic (b) and corresponding polarized fluorescence (c and d) images of a bilayer assembly PPEI/TiOPc, where a film of PPEI has been vacuum-deposited onto an annealed TiOPc surface (as in image a) and subsequently vapor-annealed for only 30 min. Topographic (e) and corresponding polarized fluorescence (f and g) images of PPEI on glass which has been vapor-annealed for 30 min. (h) Topographic image of 300 nm thick film of PPEI on glass which has been vapor-annealed for 48 h. (i) Fluorescence image of an annealed 300 nm PPEI film similar to that shown in image h.

annealing. Here topographically it can be seen that the film of nanometer scale PPEI on TiOPc (Figures 7b−d) has been transformed into needle like micron length PPEI crystals resting on TiOPc nanocrystals. Figure 8b shows an enlargement of the TiOPc region marked in Figure 8a. The surface topography of TiOPc on glass (Figure 7a) and the topography of the bare TiOPc after the secondary annealing of the PPEI over layer (Figure 8b) display comparable features. The resolution of Figure 8a is slightly better than that of Figure 7a due to a sharper near-field probe. The initial annealing of the TiOPc for 24 h, prior to vacuum deposition of the PPEI and secondary annealing, serves to crystallize the TiOPc and help maintain its topographical integrity throughout the PPEI crystallization process. The solvent-vapor-annealing process is remarkable in light of the fact that both TiOPc and PPEI are nearly insoluble in methylene chloride.

The topographical and fluorescence properties of PPEI crystals on bare glass and on a nanocrystalline TiOPc layer were

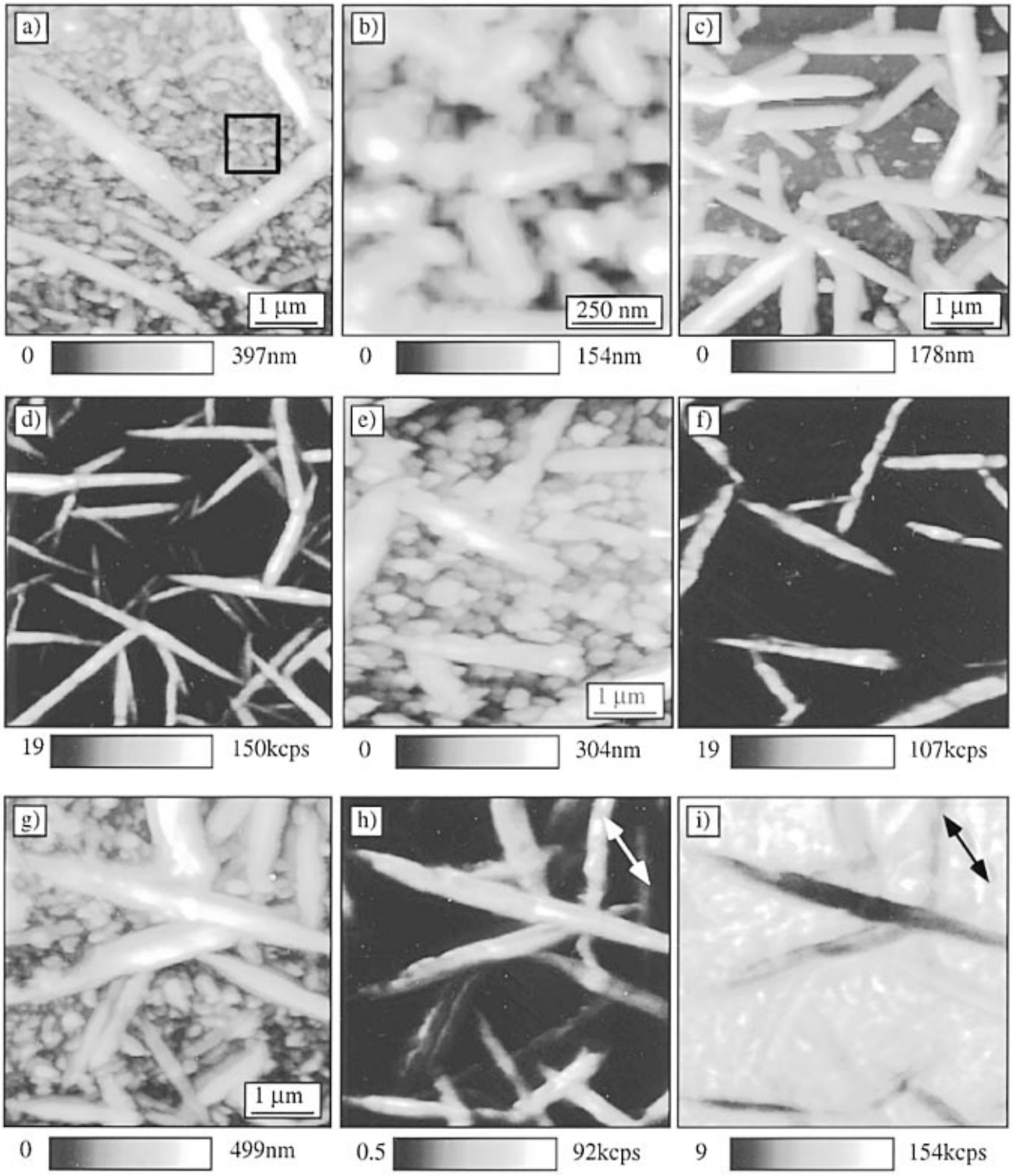

Figure 8. (a) Topographic image of a 48 h vapor-annealed PPEI film (30 nm) on a TiOPc film (10 nm). The TiOPc thin film was annealed for 24 h prior to deposition of the PPEI over layer. (b) Enlargement of the TiOPc only region marked in image a. Topographic (c) and corresponding fluorescence (d) images of a vapor-annealed PPEI film (30 nm) on glass. Topographic (e) and corresponding fluorescence (f) images of a vapor-annealed film of PPEI (30 nm) on TiOPc (10 nm). Topographic (g), fluorescence (h), and polarized transmission (i) images of a vapor-annealed thin film of PPEI (30 nm) on TiOPc (10 nm).

compared by imaging a series of regions on the same substrate. Experimental conditions (i.e. near-field probe, excitation power, tip sample distance, dither frequency, etc.) were held constant in order to make quantitative comparisons between the two environments. Figures 8c−f show typical topographical and fluorescence images from this series of experiments. Circularly polarized 488 nm light was used for photoexcitation in order to ensure equal excitation of the anisotropically absorbing PPEI crystals in a particular image area. All PPEI emission greater than 550 nm was collected at the detector. Topographically, PPEI crystals on glass and on a TiOPc layer appear smooth on their upper surface. Fluorescence from PPEI crystals on glass is relatively uniform indicating uniform crystal thickness. In contrast, the emission from the PPEI crystals on TiOPc display variations in intensity along the length of the crystal. The bottom surface of these crystals undoubtedly conforms to the

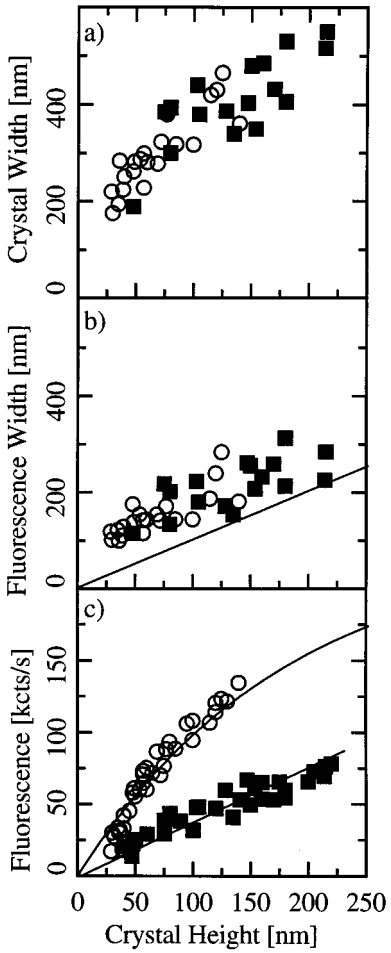

Figure 9. Plot of topographical width (FWHM), fluorescence width (FWHM), and total fluorescence intensity of PPEI crystals versus crystal height for PPEI crystals on glass (●) and PPEI crystals on TiOPc (■). The widths, heights, and fluorescence intensities were measured directly from the topographical and fluorescence images which include Figures 8c−f. Photoexcitation of the PPEI crystals was performed at 488 nm with circularly polarized light in order to ensure equal excitation of all crystals irrespective of orientation. (a) Plot of the measured topographical width versus topographical crystal height of PPEI on glass (●) and PPEI on TiOPc (■). (b) Plot of the fluorescence width versus topographical crystal height. (c) Plot of the fluorescence intensity (cps) versus PPEI crystal height for PPEI on glass (●) and PPEI on TiOPc (■). The fluorescence intensity was measured as the average intensity in ∼100 nm by ∼500 nm regions.

topography of the smaller TiOPc crystals. The nonuniformity of the thickness of the PPEI crystals likely results in the observed variations in the fluorescence intensity along the length of the crystals.

The width and height of the PPEI crystals can be obtained by an analysis of both the topographical and fluorescence images. The width of the fluorescence features in Figures 8d and 8f are clearly narrower than their topographical counterparts in Figures 8c and 8e, respectively. Figure 9a shows a plot of crystal width versus crystal height in nanometers measured topographically for a number of crystals. The vertical heights of the PPEI crystals are accurately represented to within 0.5 nm in the topographical image. The average height of crystals grown on TiOPc is 150 nm, whereas the average height of the crystals grown on bare glass is 80 nm. However, the topographical images do not accurately represent the width of the crystal. This is a common problem with scanning probe techniques where large diameter probes are used to image tall objects. The PPEI crystals appear wider in the topographical image since they represent a convolution of the shape of the tip and the shape of the crystal. The near-field optical images, in contrast, more accurately depict the width of the crystals since the NSOM aperture is smaller than the width of the crystals. Figure 9b shows a plot of fluorescence width versus crystal height in nanometers. The average width of crystals grown on TiOPc is 200 nm, while the average width of crystals grown on glass is 180 nm. Figure 9b accurately represents the width of PPEI crystals as function of crystal height. The nearly 1:1 increase in height with width shows that the crystals are nearly square in profile.

Polarized Spectroscopic NSOM Experiments. The fluorescence from the low energy CT state of the PPEI crystals is highly polarized, and the maximum fluorescence intensity occurs at an angle of the ∼45° from the long axis of the crystal. The emission dipole of this low energy CT state appears to be nearly coincident with the absorption dipole of the higher energy S_1 state. Figures 10a,b display the polarized fluorescence images of a collection of PPEI crystals on glass obtained with 488 nm circularly polarized photoexcitation. Depending on the orientation, the emission from a PPEI crystal may appear in only one of the images. If the emission dipole of a crystal is aligned at 45° with respect to parallel and perpendicular detectors, then the crystal will appear in both images.

Linearly polarized light can be used to selectively photoexcite the PPEI crystals. Figure 10c,d are the polarized fluorescence images of PPEI crystals on a TiOPc surface obtained with 488 nm light polarized vertical to the image. The incident light is not perfectly polarized in the vertical direction, which results in a small component of excitation in the horizontal direction. The absorption dipole of the crystal in the upper region of Figure 10c is nearly coincident with the incident 488 nm vertically polarized light. Consequently bright emission is observed for this crystal. Contrastingly, the lower crystal shows very little emission since its absorption dipole is nearly orthogonal to the excitation. The orthogonally polarized fluorescence image, Figure 10d, shows increased fluorescence intensity from the lower crystal since the emission dipole is nearly coincident with the horizontal direction.

The large anisotropic absorption of the PPEI crystals is also apparent in the transmission NSOM images of the PPEI and PPEI/TiOPc samples. It has been shown that the dominant contrast mechanism of transmission near-field spectroscopy, for samples that are imaged at a wavelength that corresponds to a strong absorption, is absorption of the near-field.[33] Thus, the transmission NSOM image is essentially a measure of the spatially resolved extinction (absorption) of the sample. However, transmission NSOM is complicated by the competition between (i) the absorption of the near-field light by the sample (which is reflected in an intensity decreases of the far-field light at the detector) and (ii) refractive index effects in the sample/probe near-field region (which is reflected in increases and decreases of the detected far-field light due to the scattering of the near-field light).[33] Refractive index effects are the dominate contrast mechanism in transmission NSOM images for probe wavelengths that are not "in resonance" with a strong absorption band of the sample. Furthermore, even for situations where the probe wavelength does correspond to a strong absorption of the medium, the refractive index effects can dominate if the polarization direction of the NSOM probe is orthogonal to the absorption dipole of a sample in the region being probed.

These complex effects are demonstrated in Figure 8i for PPEI/TiOPc. The highly anisotropic absorption of light by the crystals is nicely displayed by the nearly parallel crystals showing opposite transmission characteristics. This results from one

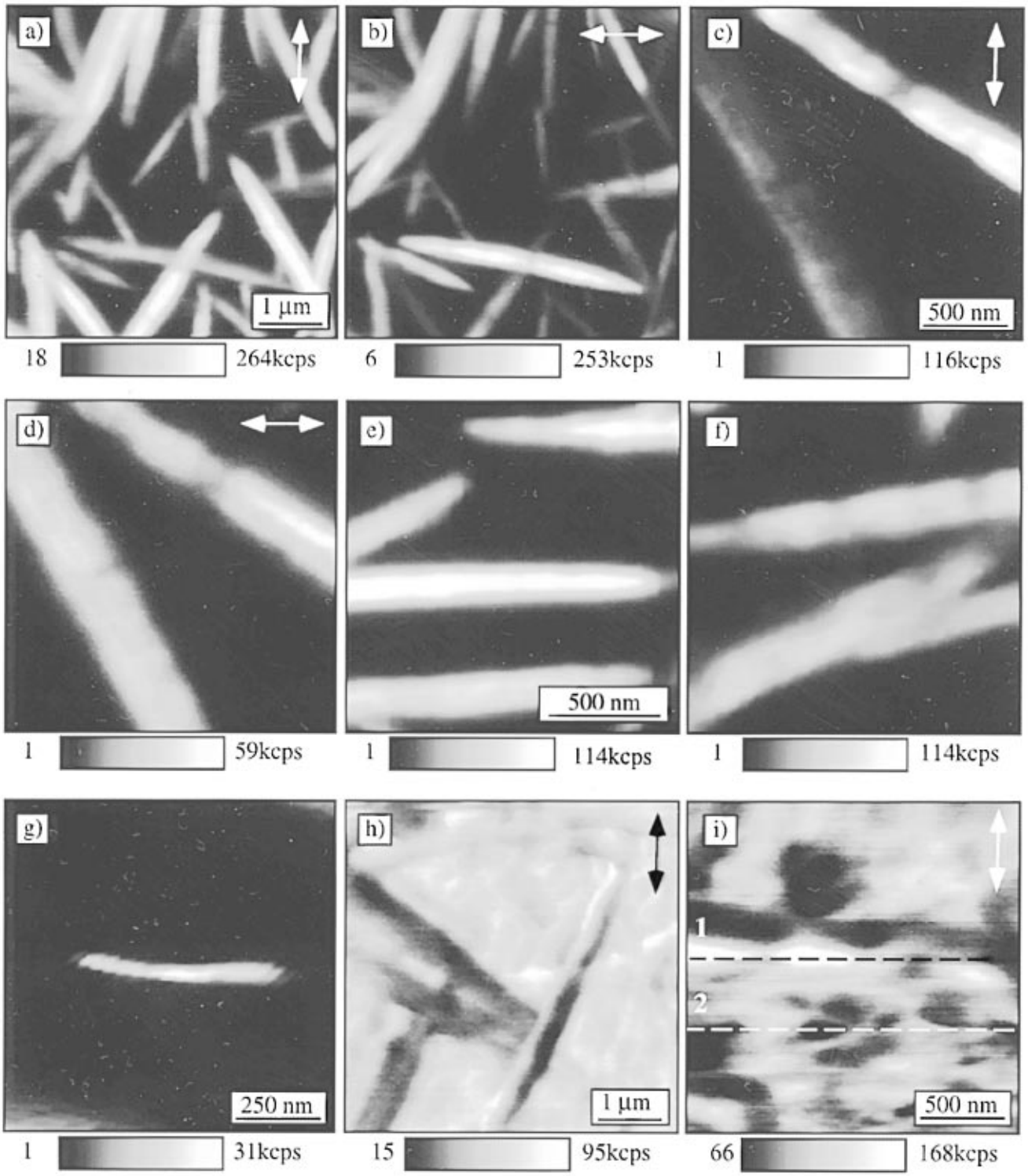

Figure 10. Polarized near-field fluorescence images (a and b) of the PPEI crystals on glass obtained following photoexcitation with 488 nm circularly polarized light. Polarized near-field fluorescence images (c and d) of PPEI crystals on TiOPc obtained following photoexcitation with 488 nm linearly polarized light in the direction vertical to the images. Fluorescence images of PPEI crystals on glass (e) and PPEI on TiOPc (f). Images (e and f) are plotted on the same scale in order to reveal the quenching of the PPEI fluorescence by the TiOPc underlayer. (g) High resolution fluorescence image of a small PPEI crystal on TiOPc. (h) Polarized 633 nm near-field transmission image of PPEI crystals on TiOPc crystals. (i) Polarized 820 nm near-field transmission image of a PPEI crystal on TiOPc. Line 1 in i is along the top of the PPEI crystal. Line 2 is along a region of TiOPc nanocrystallites only. The line scan plots corresponding to lines 1 and 2 are shown in Figure 12.

crystal being "upside down" with respect to the other. The maximum absorption of the PPEI crystals occurs at ~45° off of the long axis of the crystal. The dark regions in Figure 8i apparently correspond to contrast due to absorption of the near-field of the probe. However, when crystals are thin or when the transition dipole and excitation polarization are not coaligned, anisotropic refractive index effects become more important and in some cases may even become the dominant contrast mechanism for the transmission image. For example, thin crystals of PPEI and crystals that are not coaligned with the excitation polarization appear as bright regions in Figure 8i. The intensity of light coupled to the detector over these crystals is nearly the same as that observed over the nonresonant TiOPc regions of the image. It might appear as if little or no light is being

absorbed by these crystals. However, clearly these crystals are absorbing light since the corresponding fluorescence image shows that light is emitted from these regions of the film.

Nanoscale Structure of the Interface. In this section, insights into the nanoscale structure of the PPEI/TiOPc interface are obtained by carefully analyzing a variety of polarized fluorescence and transmission NSOM experiments. These experiments address to what extent the PPEI layer conforms to the TiOPc underlayer and leads to an estimate of the nature and spatial distribution of the contact points between the layers. The results take advantage of transmission NSOM at multiple probe wavelengths which allows for an examination of the TiOPc underlayer, while locating the tip over PPEI crystals. The use of multiple probe wavelengths is also an aid in interpreting the complex contrast mechanisms that are present in the transmission images.

The spatial variation in thickness of the PPEI crystals on TiOPc has been probed by measuring the transmission of 488 nm light through the sample. Topographic, polarized transmission, and fluorescence optical images of the PPEI/TiOPc assembly obtained with 488 nm linearly polarized light are shown in Figures 8g−i. The direction of polarization of the 488 nm incident light is shown in the Figure 8i. At 488 nm the PPEI crystals absorb strongly while TiOPc has little or no absorption. The polarization has been adjusted so as to maximize absorption on the large nearly horizontal PPEI crystal near the top of Figure 8i, in order to control and in some cases minimize the complex contrast effects that were described in the previous section.

The fluorescence and transmission images are complementary, i.e. regions of strong absorption in Figure 8i correspond to regions of strong emission in Figure 8h. Figures 8h,i, as well as other images not presented here, demonstrate that the local variations in fluorescence intensity along single PPEI crystals (dark spots) are due to local variations in the crystal thickness (thin spots). Since the upper surface of the PPEI crystals are flat (Figure 8g), the thin spots in PPEI must be due to the lower surface of the crystal conforming to the nanocrystalline TiOPc surface. In other words, the dark spots in the fluorescence correspond to locations where a relatively large TiOPc crystal protrudes up into the PPEI/TiOPc interface. Presumably, these dark spots indicate some of the electrical contact points between the PPEI crystal and the nanocrystalline TiOPc surface.

A simple qualitative model of thin, highly annealed PPEI/TiOPc interfaces is shown in Figure 11a. This model is consistent with the various NSOM topographic, fluorescence, and transmission data presented in this paper. The interface is comprised of relatively large PPEI crystals with small nanocrystals of TiOPc making occasional contacts with the PPEI. The individual contacts are only on the order of a few tens of nanometers, in most cases. Much of the underside of the PPEI crystal is free of TiOPc contacts. Occasionally, larger TiOPc crystals jut up into the PPEI crystals. The impact of such an interface on the fluorescence quenching and efficiency of the PPEI/TiOPc heterojunction is discussed in the following section.

Polarized transmission NSOM at wavelengths of 633 nm (Figure 10h) and 820 nm (Figure 10i) have been performed in order to further probe the nanocrystalline TiOPc layer, and specifically, the TiOPc crystals that are located beneath the PPEI crystals. 820 nm light is resonant with the CT transition of the TiOPc while PPEI is nonabsorbing at this wavelength. Figure 10i shows a polarized transmission image of a PPEI crystal (center of image, horizontally oriented) on the TiOPc surface, where the incident 820 nm light is polarized vertical to the image. Decreased transmission results from resonant absorption

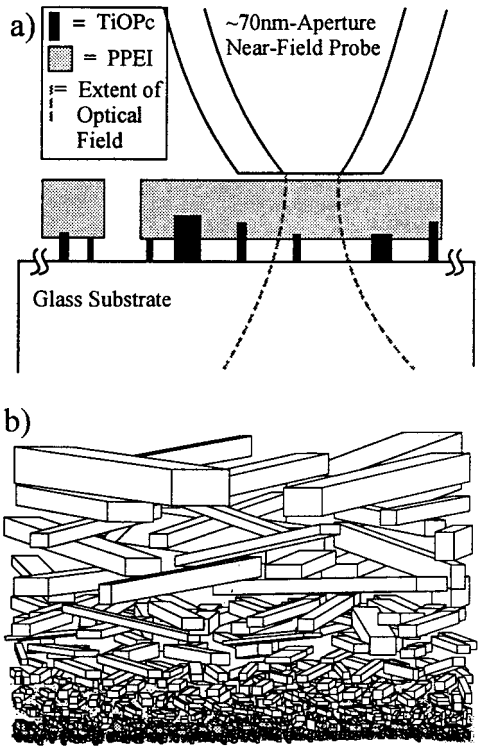

Figure 11. (a) Schematic representation of near-field probe, the optical field, and the nanocrystalline PPEI/TiOPc interface, drawn approximately to scale. (b) Depiction of a thick PPEI layer, solvent-vapor-annealed for a short amount of time, showing a gradient of crystal sizes toward the interface from micron size to amorphous.

of the 820 nm light by the TiOPc crystals. This image and its horizontally polarized counterpart (not shown) reveal polarization dependent features in the transmitted light intensity due to anisotropic absorption of the TiOPc. These variations are apparent in TiOPc-regions of the sample. More importantly, these variations are also observed in the region covered by a PPEI crystal. This is a critical result that strongly suggests that the TiOPc layer underneath a PPEI crystal is similar in structure to the exposed TiOPc regions. Line scan plots of the vertical and horizontal transmission intensities are plotted in Figure 12. The relative change in transmission intensity as a function of distance along the horizontally oriented PPEI crystal (line 1, Figure 10i) for both polarizations is plotted in Figure 12a. Figure 12b shows line scan plots of the polarized transmission in a region of TiOPc only (line 2, Figure 10i). Clearly the magnitude of the intensity variations are comparable over the PPEI crystal and over TiOPc only.

Unfortunately, the transmission images are complicated by contrast mechanisms other than the anisotropic absorption of the TiOPc nanocrystals. For example there is increased intensity above the PPEI crystal due presumably to increased scattering from the near-field to the far-field as a result of a higher refractive index in the PPEI crystal compared to the TiOPc-coated substrate. The dark upper edge on the PPEI crystal is apparently a tip-type NSOM/topographical artifact that has been described in detail for other crystals.[35] The artifact results from the large radius of the near-field probe which causes the sample to retract away from the tip as the edges of tall crystals are encountered. This, in turn, briefly increases the distance between the aperture and the sample at the crystal edge. Consequently at the edge of the crystal less light is diffracted from the near-field to the far-field, and the edges of the crystal appear as dark lines in the transmission image.

Figure 10h shows a polarized transmission image obtained

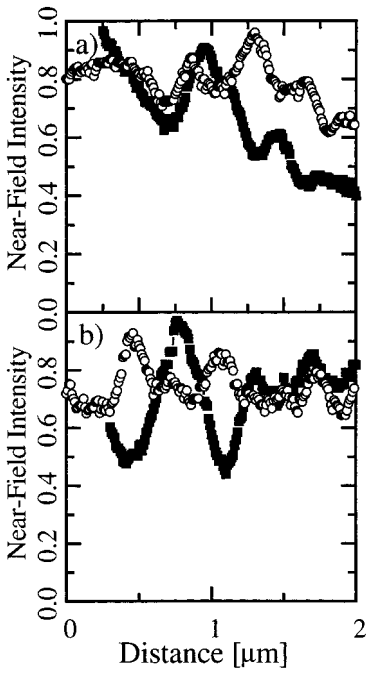

Figure 12. (a) Line scan plot of the polarized NSOM intensity variations along the PPEI crystal in Figure 8i (line 1) obtained with linearly polarized 820 nm light. (b) Line scan plot of the polarized NSOM intensity variations along a region of TiOPc crystals only shown in Figure 8i (line 2). Transmission data obtained with (○) horizontally and (■) vertically polarized 820 nm light.

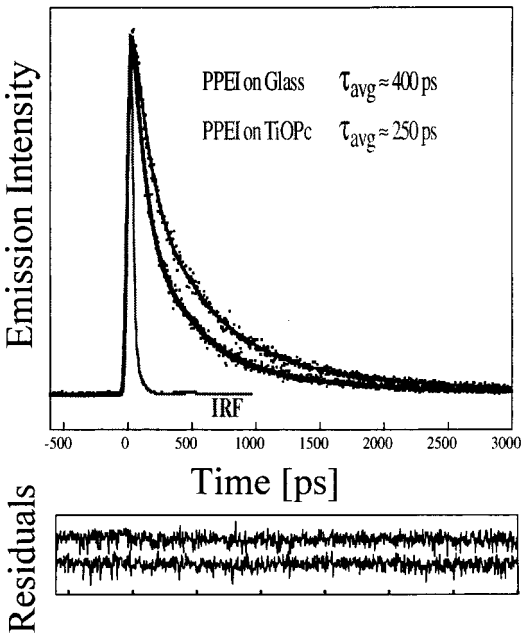

Figure 13. Near-field fluorescence decay curves for single PPEI crystals on bare glass and on a nanocrystalline TiOPc surface. The instrument response function is plotted at time zero. The solid lines through the data represent a convolution of the IRF with an exponential decay of the form $I = A_1 \exp[t/\tau_1] + A_2 \exp[t/\tau_2] + A_3 \exp[t/\tau_3]$. The lifetime of fluorescence on glass is $\tau_{avg} = 400$ ps ($\tau_1 = 130$ ps $A_1 = 1013$, $\tau_2 = 493$ ps $A_2 = 872$, $\tau_3 = 1654$ ps $A_3 = 154$) compared to $\tau_{avg} = 252$ ps ($\tau_1 = 82$ ps $A_1 = 880$, $\tau_2 = 352$ ps $A_2 = 530$, $\tau_3 = 1309$ ps $A_3 = 92$) on TiOPc.

with 633 nm light of PPEI crystals on TiOPc. 633 nm light is simultaneously resonant with the low energy CT excitonic transition of PPEI and the high energy transition of TiOPc. In this image the PPEI crystals appear dark due to polarized absorption from the CT band. Interestingly, the polarization direction of this band is parallel to the S_1 Frenkel band which is probed by the 488 nm NSOM images.

Static and Time-Resolved NSOM Fluorescence Quenching Measurements. The fluorescence intensity as a function of crystal height was measured directly for individual crystals of PPEI. A series of fluorescence images were taken of PPEI crystals on bare glass and on the nanocrystalline TiOPc quencher. Figure 9c shows a plot of the fluorescence intensity versus crystal height for the quenched and unquenched films for a number of PPEI crystals. The average fluorescence intensities of PPEI crystals were measured in rectangular areas of ~100 nm by ~500 nm, along regions of constant vertical height. This average intensity was used to account for the local variations in emission intensity due to local variations in thickness of the PPEI crystals. The fluorescence intensity of the unquenched PPEI crystals on glass is expected to increase exponentially with crystal thickness as the optical density at 488 nm of the PPEI crystals increases. The solid line through the unquenched fluorescence data represents a fit of the data to $I = I_{max}(1 + e^{-\alpha l})$ using the measured optical extinction coefficient $\alpha_{488} = 5.5 \times 10^4$ cm^{-1} for PPEI at 488 nm. The solid line through the quenched fluorescence is added in order to guide the eye. Figure 9c provides clear evidence of substantial quenching of fluorescence by the TiOPc layer. There is an ~60% decrease in fluorescence intensity from the PPEI crystals on the quencher as compared to the nonquencher area. The magnitude of fluorescence quenching seen for these single crystals is comparable to that observed in the far-field measurements on bulk films.[25] Unfortunately, we were unable to obtain PPEI crystals larger than 250 nm, and consequently the limited data set precludes the fitting of the data to an exciton diffusion theory.

Near-field time resolved single photon counting experiments further corroborate that quenching of PPEI fluorescence occurs on the TiOPc surface. Figure 13 shows the near-field fluorescence decays of single crystals of PPEI on glass and on TiOPc. The decay curves are well represented by a fit to 3 exponentials. The solid lines represents a convolution of the instrument response function (50 ps FWHM) with an exponential decay of the form $I = A_1 \exp[t/\tau_1] + A_2 \exp[t/\tau_2] + A_3 \exp[t/\tau_3]$. The lifetime of fluorescence on glass is $\tau_{avg} = 400$ ps ($\tau_1 = 130$ ps $A_1 = 1013$, $\tau_2 = 493$ ps $A_2 = 872$, $\tau_3 = 1654$ ps $A_3 = 154$) compared to $\tau_{avg} = 252$ ps ($\tau_1 = 82$ ps $A_1 = 880$, $\tau_2 = 352$ ps $A_2 = 530$, $\tau_3 = 1309$ ps $A_3 = 92$) on TiOPc. The error in these lifetimes is ~50 ps. This 40% decrease in emission lifetime is consistent (within experimental error) with the observed 60% decrease in emission intensity of the near-field steady state fluorescence of single PPEI crystals on glass vs TiOPc. The decrease in both lifetime and emission yield should, therefore, be attributed to a change in the nonradiative decay rate (presumably charge transfer) of the exciton state, as opposed to variations in the radiative rate.

Quenching of fluorescence occurs, surprisingly, nearly uniformly along micron length regions of PPEI crystals, even though there are multiple TiOPc contact points at the interface. Fluorescence images plotted on the same intensity scale, of PPEI crystals on bare glass, Figure 10e, and PPEI crystals on nanocrystalline TiOPc, Figure 10f, dramatically display this effect. The bright horizontal crystal in Figure 10e and the crystals shown in Figure 10f are all of ~100 nm vertical height. Figure 10g shows the fluorescence image of a small crystal of PPEI embedded on a layer of TiOPc nanocrystals. The emission intensity along the length of this crystal is uniform. We do not observe light and dark regions of emission from this crystal

Table 1. Bulk Film % Fluorescence Quenched as a Function of Solvent-Vapor-Annealing Time for Bilayer Films of PPEI/TiOPc[a,b]

PPEI annealing time	22 nm PPEI layer	48 nm PPEI layer	200 nm PPEI layer	820 nm PPEI layer
0	95	79	47	27
1 min	91	72	54	26
1 h	88	65	80	49
24 h	65	67	76	77

[a] 30 nm TiOPc films solvent-vapor-annealed for 2 h in CH_2Cl_2 prior to evaporation of the PPEI layer, were used in all cases. [b] Percent fluorescence quenched was calculated from $(1 - (Fl_{quenched}/Fl_{unquenched}))\cdot 100$, where $Fl_{quenched}$ is the fluorescence from the PPEI/TiOPc film and $Fl_{unquenched}$ is fluorescence from the PPEI film on bare glass of corresponding PPEI thickness.

even though the crystal is literally embedded on the nanocrystalline TiOPc layer.

The absence of high-contrast dark spots in the fluorescence NSOM images is apparently a consequence of the extremely small ($<\sim$100 nm^2) contact areas for each TiOPc crystal that is in contact with the PPEI. This is shown schematically in Figure 11a. Excitons created in the near-field of the probe must diffuse to a contact point in order to be quenched. Since the contact areas are exceedingly small and widely spaced relative to the size of the contacts, many excitons can migrate parallel to the plane of the interface over micron lengths without finding a TiOPc contact. Thus, the relatively uniform quenching efficiency, even for thin crystals, is a consequence of the spatial distribution of the contact points and the three-dimensional nature of the exciton migration.

Solvent Annealing and Fluorescence Quenching Efficiencies. Further insights into the effect of the solvent-vapor-annealing on fluorescence quenching efficiency are found in the bulk-film fluorescence quenching experiments of Gregg *et al.*[25] In those studies, PPEI films of varying thickness on various *p*-MSL layers were prepared and the exciting light was incident on the air/PPEI interface. The excitons created on the top PPEI surface must traverse the PPEI layer in order to become quenched at the PPEI/*p*-MSL interface. The fluorescence intensity as a function of film thickness was analyzed to obtain a measure of the diffusion length of at least 2.5 μm for the highly efficient quencher, poly(methylthiophene) (PMT). The fluorescence of thin PPEI films (<200 nm) were nearly completely quenched by the PMT layer, while much thicker PPEI films were less efficiently quenched due to the longer required exciton transit times to the interface and the consequent "energy wasting" *en route* to the interface. In contrast, PPEI/TiOPc bilayers showed inefficient quenching ($\sim$40−60%) even for very thin PPEI layers. The NSOM results summarized in Figure 11a would suggest that inefficient fluorescence quenching observed for bulk films should be attributed to poor contact between PPEI/TiOPc at the interface that resulted from restructuring of the interface during solvent annealing.

Analogous arguments to those presented above that explain the spatial uniformity of PPEI/TiOPc fluorescence quenching also qualitatively account for the low quenching efficiency. Thus, even for a very thin PPEI layer (for which exciton migration perpendicular to the interface should be facile) the excitons are not efficiently quenched since the migration parallel to the interface is still required in order to find a contact point with TiOPc. For PPEI on PMT, the quenching efficiencies are nearly 100% for thin films, presumably due to a more effective contact at the PPEI/PMT interface. The cross-linked PMT layer is likely not restructured by solvent-vapor-annealing.

Additional evidence that extensive solvent-vapor-annealing of thin PPEI/TiOPc interfaces disturbs the interfacial region is shown in Table 1. Here the fluorescence quenching efficiency of various bulk samples has been measured as a function of solvent vapor-annealing time. For thin PPEI layers on top of thin TiOPc layers, the quenching efficiency is nearly 100% for bilayers with a PPEI layer which has not been annealed. Even a small amount of annealing reduces the efficiency of quenching due, presumably to the restructuring of the PPEI/TiOPc interface.

It is important to note that in contrast to the observed behavior for the 22 nm and 48 nm PPEI films, the thicker films actually show an increase in fluorescence quenching efficiency due to solvent annealing. This contradictory behavior can be rationalized by considering the topographical images of thick PPEI films (Figure 7h) and the schematic drawing of such a film in Figure 11b. For thick films, solvent-vapor-annealing improves the upper regions of the PPEI layer without disturbing the interface regions. This improves energy migration to the PPEI/TiOPc interface without degrading the contact regions between the PPEI and TiOPc layers at the interface.

Conclusions and Summary

The high topographic and optical resolution of NSOM has been employed to spatially resolve the complex morphologies, spectroscopy, and charge transfer induced fluorescence quenching efficiencies of a PPEI/TiOPc bilayer assembly. NSOM topographic, fluorescence, and transmission images have been used to show that the highly solvent-vapor-annealed PPEI/TiOPc interface is comprised of relatively large PPEI crystals with small nanocrystals of TiOPc making occasional contacts with the PPEI. Only a small fraction of the area of the interface makes good contact between the bilayers, and the contact regions are less than 100 nm^2 in most cases. Moreover, transmission NSOM has shown that the nanocrystalline TiOPc layer underneath PPEI crystals is similar in structure to the exposed TiOPc regions. Fluorescence of PPEI is quenched by $\sim$60% on the TiOPc surface and has been shown to occur, surprisingly, nearly uniformly along micron length regions of PPEI crystals, even though there are multiple TiOPc contact points at the interface. This relatively uniform quenching efficiency, even for thin crystals, is proposed to be a consequence of the spatial distribution of the extremely small ($<\sim$100 nm^2) contact points and the three-dimensional nature of the exciton migration. The restructuring of the PPEI/TiOPc interface in *thin films* by solvent-vapor-annealing has been shown to reduce the efficiency of charge transfer induced fluorescence quenching at the interface. On the other hand, annealing of *thick films* of PPEI has been shown improve the efficiency of quenching by inducing crystallinity at the outer surface, and consequently improving energy migration toward the PPEI/TiOPc interface, without degrading the efficient amorphous contact region between the PPEI/TiOPc at the interface.

Acknowledgment. The research at Minnesota was supported by the National Science Foundation and the Office of Naval Research. A.Z. and B.A.G. gratefully acknowledge support from the U.S. Department of Energy/OER/BES Chemical Sciences Division.

Supporting Information Available: A more detailed description of the thin film X-ray diffraction measurements, and a table of Miller indices, single crystal calculated *d*-spacings, thin film observed *d*-spacings, and thin film diffraction peak assignments, are given in S1−S5 (5 pages). See any current masthead page for ordering and Internet access instructions.

JA9717774